Seismic analysis of offshore wind turbines on bottom-fixed support structures with soil-structure interaction

SEISMIC ANALYSIS OF OFFSHORE WIND TURBINES ON BOTTOM-FIXED SUPPORT STRUCTURES

Natale Alati, Giuseppe Failla and Felice Arena

Department of Civil, Energy, Environmental and Materials Engineering (DICEAM)

University of Reggio Calabria

Via Graziella, Località Feo di Vito, 89124 Reggio Calabria, Italy

ABSTRACT

This study investigates the seismic response of a horizontal axis wind turbine on two bottom-fixed support structures for transitional water depths (30-60 m), a tripod and a jacket, both resting on pile foundations. Fully-coupled, non-linear time-domain simulations on full system models are carried out under combined wind-wave-earthquake loadings, for different load cases, considering fixed and flexible foundation models. It is shown that earthquake loading may cause a significant increase of stress resultant demands, even for moderate peak ground accelerations, and that fully-coupled non-linear time-domain simulations on full system models are essential to capture relevant information on the moment demand in the rotor blades, which cannot be predicted by analyses on simplified models allowed by existing standards. A comparison with some typical design load cases substantiates the need for an accurate seismic assessment in sites at risk from earthquakes.

KEYWORDS

Seismic Analysis, Offshore Wind Turbine; Tripod; Jacket; Flexible Foundation

1. INTRODUCTION

While an increasing number of offshore wind farms are being planned worldwide to satisfy a growing energy demand, the design of offshore horizontal axis wind turbines (HAWTs) is facing

novel and challenging tasks. In this context, seismic assessment has become crucial for bottom-fixed offshore HAWTs in seismically active areas, especially since evidence exists that earthquakes can damage the support structure of land-based HAWTs, as in the case of the 1986 North Palm Springs Earthquake [1].

Seismic assessment of offshore HAWTs is prescribed by recent international guidelines and standards [2-5]. In general, fully-coupled non-linear time-domain simulations [2-5] or response spectra methods [2-5] are suggested, on either simplified [2,5] or full system models [4]. Fully-coupled non-linear time-domain simulations compute the response to earthquake and environmental loads acting simultaneously, considering interactions of aerodynamic, hydrodynamic and seismic responses [2-5], while response spectra methods involve a linear superposition of separately computed responses to earthquake and environmental loads [2-5]. Simplified system models include the support structure only, with the rotor-nacelle assembly (RNA) modelled as a lumped mass at the tower top [2,5]. Full system models involve the support structure and the whole turbine, i.e. nacelle, rotor blades and, in general, turbine components such as power transmission inside the nacelle, pitch and speed control devices, with a different degree of accuracy depending on the specific modelling adopted [4]. Fundamental load cases reflect the possible scenarios for an earthquake strike, and are generally chosen as: (1) earthquake loads with operational loads, i.e. earthquake striking while the rotor is spinning; (2) earthquake loads with emergency stop loads, i.e. earthquake triggering a shutdown; (3) earthquake loads with non-operational loads, i.e. earthquake striking when the turbine is parked (not operating), due to wind speeds exceeding the cut-off wind speed of the turbine.

Since seismic assessment of offshore HAWTs has been included in international guidelines and standards, there is a great interest in assessing to which extent stress demands are increased by earthquake loads, and whether numerical results may be significantly affected by the method of analysis and system modelling adopted. Extensive research studies on these issues are not available yet. However, it is important to remark that earlier studies on land-based HAWTs have already

addressed these issues, showing that accurate predictions of the seismic response can be obtained only by performing fully-coupled non-linear time-domain simulations, on full system models including support structure and the whole turbine [6-11]. The main reasons substantiating these conclusions can be summarized as follows. A full system model allows loads acting on all system components to be estimated, including those on the rotor blades, whose integrity is crucial to ensure a reliable power production over the design life of the HAWT. Further, higher rotor modes can be considered only in a full system model, and these modes may be important in the seismic response, as they may fall in the region of maxima spectral accelerations [8-10]. Non-linear time-domain simulations can capture how tower top oscillations due to the earthquake ground motion affect rotor aerodynamics, in particular the relative wind speed at the blades, depending on which the aerodynamic loading, i.e. lift and drag forces on the blades, are calculated. Also, important sources of non-linearity have been found in soil response, especially when HAWTs are installed on relatively soft soils or loose soils containing alluvial deposits [12]. Within this theoretical framework, Zhao et al. [6-7], Prowell et al. [8-11] have investigated the seismic response of land-based HAWTs of different rated power, by fully-coupled non-linear time-domain simulations on full system models of the HAWT, based on a hybrid multi-body system approach [6-7] or a combined modal and multi-body dynamics formulation, as implemented in FAST software package [8-11]. Zhao et al. have found that force and bending moment at the tower base of a 1.5MW HAWT are affected considerably by an earthquake striking in the operational state, especially in the lateral direction where there are no wind loads, even for a weak earthquake intensity [6]. Prowell et al. have shown that, for the reference National Renewable Energy Laboratory (NREL) 5MW HAWT [13], the bending moment demand at the tower base is significantly above the demand from extreme wind events. This result has been obtained for parked, operational and emergency stop simulations under a large set of ground motions [9-10], showing that earthquake loads may be design driving for large turbines in regions of high seismic hazard.

It is apparent that the conclusions above, as drawn from the seismic analysis of land-based HAWTs, have general validity and shall be kept in mind also for seismic assessment of offshore HAWTs. On the other hand it is important to remark that, in this case, non-linearities arise also from the hydrodynamic loading and that, in general, interactions of aerodynamic, hydrodynamic and seismic responses shall be considered in fully-coupled, non-linear time-domain simulations.

Studies on the seismic response of offshore HAWTs are not as numerous as those on land-based HAWTs. They are quite recent and have been concerned with offshore HAWTs on monopiles. Hacifiendoglu [14] has investigated the seismic response of a 3MW HAWT on a monopile, under a stochastic earthquake excitation occurring in the parked state. A simplified model of the HAWT has been used, with the RNA modelled as a lumped top mass and a full 3D model of sea water and soil, and motion equations of the coupled system water-structure-soil have been derived upon enforcing continuity of displacements in the normal direction to the interfaces. Sensitivity of displacement and stress responses to sea water level, soil conditions and presence of a surrounding ice sheet has been investigated. Kim et al. [15] have studied the seismic response of the NREL 5MW HAWT on a monopile, under real and artificial earthquake ground motions occurring in the parked state. A simplified model of the HAWT has been implemented, with the RNA modelled as a lumped top mass; non-linear springs have been introduced along the pile length to model soil stiffness, considering also the variation of the earthquake ground motion through different soil layers. Important conclusions of this study are that fragility curves of the HAWT, built for a variety of peak ground accelerations (PGAs), can be predicted reasonably well by static pushover analyses and, also, that variation of earthquake ground motion through different soil layers plays an important role in the estimation of the fragility curves.

The purpose of this paper is to investigate the seismic behaviour of bottom-fixed offshore HAWTs in transitional water depths (30-60 m). This subject appears of particular interest considering that wind farms are being planned far from near-shore shallow waters (< 30 m) to minimize visual impact, and there are transitional water depth sites with high wind speed resources

and medium-to-high seismic hazard. Typical examples in the U.S. can be found in the Hawaiian islands [16-17]. In particular, the study is carried out on the NREL 5MW HAWT, as mounted on two typical steel support structures for transitional water depths, a tripod and a jacket resting on pile foundations. Wind and wave environmental states, water depth and soil profile are set in agreement with similar theoretical studies on offshore HAWTs [18-19]. Consistently with the approach followed for land-based HAWTs [9-11], the seismic response is investigated for a set of real earthquake records taken from existing databases [20-21], with different frequency content and intensity. Fully-coupled non-linear time-domain simulations are carried out on full system models including non-linear soil stiffness, using BLADED software package [22], certified by Germanischer Llyod for design of wind turbines. Simulations are run for earthquake striking in operational and parked states, and earthquake triggering an emergency stop, comparing stress resultant demands to those when no earthquake loads are considered, for fixed and flexible foundation models (FMs). For a further insight into the importance of seismic assessment, a comparison with demands from some typical design load cases prescribed by IEC 61400-3 is also provided [3].

The paper is organized in six Sections. Support structures and load cases are presented in Section 2 and Section 3. Typical features of the response to an earthquake strike are illustrated in Section 4. Results of time-domain simulations with the full earthquake set are described in Section 5, while the comparison with some IEC 61400-3 load cases [3] is discussed in Section 6.

2. TRIPOD AND JACKET SUPPORT STRUCTURES

The turbine is the NREL 5MW three-bladed turbine, whose details can be found in ref. [13]. Two different steel support structures are considered, as shown in Figure 1: one with a centre column tripod, and the other with a jacket quattropod, both resting on pile foundations. The two support structures are designed according to current practice; in particular, the one with the jacket quattropod is identical to that studied in ref. [23]. Details on the structural members are given in

Figure 2. It is assumed that the water depth is 50 m, and the reference three-layer sandy soil of the OC3 project [18-19] is considered. In the following, the two support structures will be referred to as "Tripod" and "Jacket", for simplicity.

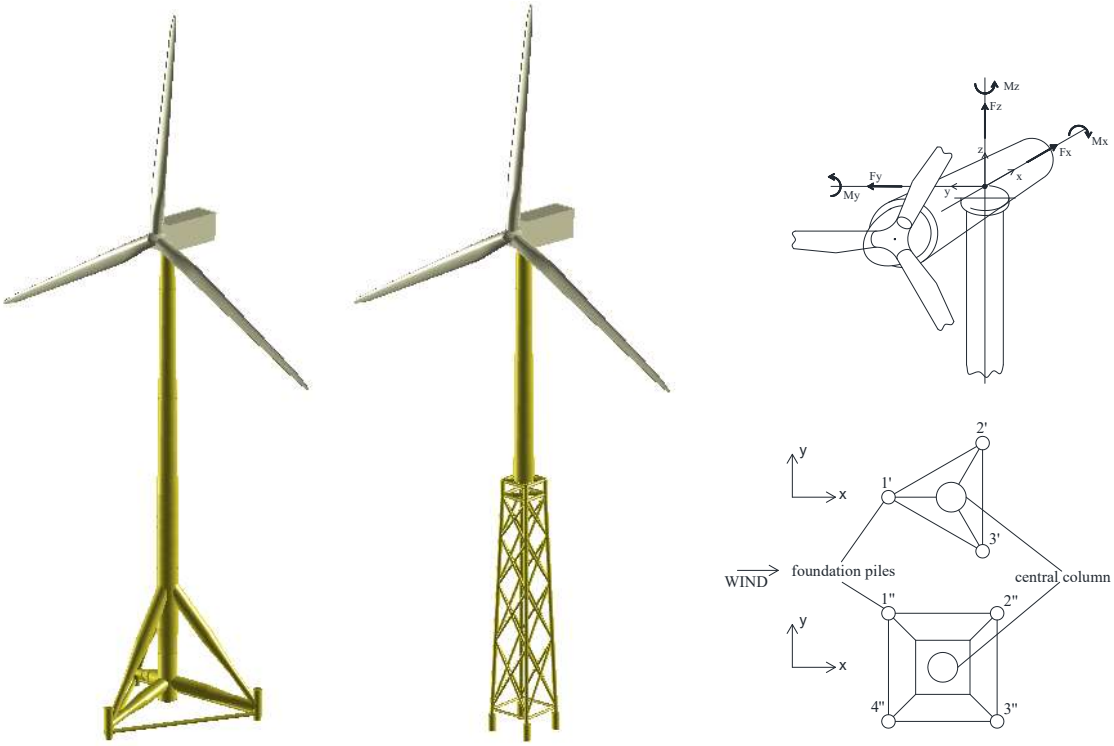

Figure 1. Tripod and jacket support structures, pile foundations and positive stress resultants.

The full system is implemented in BLADED [22], modelling nacelle, blades, drive train, control system, as given in ref. [13]. Beam elements with shear deformation are used for support structure structural members, piles and blades. Steel parameters are: Young's modulus = 210 GPa, Poisson coefficient = 0.3, Mass density = 7850 kg m^{-3}. Two different FMs are considered: the first is fixed (clamped base), the second is flexible with lateral horizontal and vertical springs along the piles at a 1 m spacing, and a vertical spring at the piles tip, modelling soil stiffness [18-19, 24-25] (with respect to the reference system in Figure 1, horizontal springs are in x and y directions, vertical springs in z direction). All springs are supposed to be uncoupled, with non-linear force-displacement laws set based on the p-y, t-z and Q-z curves in the API code [26], using the

parameters of the OC3 project three-layer sandy soil [18-19] and following the prescriptions for layered soils given in ref. [19] (detailed examples can be found also at the NREL website: https://wind.nrel.gov/forum/wind/viewtopic.php?f=3&t=880&start=0). For completeness, *p-y*, *t-z* curves at various depths along the piles, and the *Q-z* curve at the piles tip, are reported in the Electronic Supplementary Material (ESM) attached to the paper.

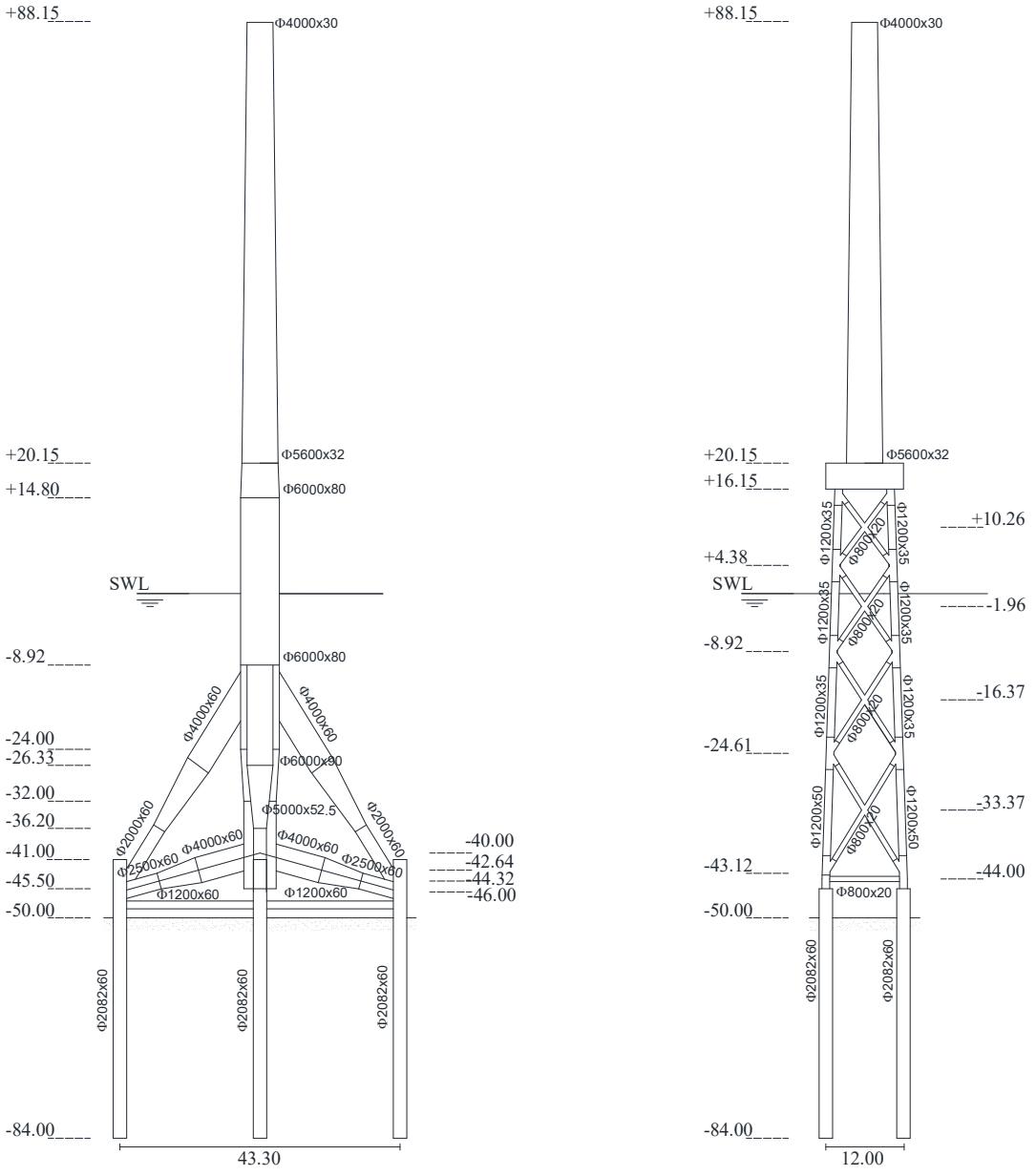

Figure 2. Geometry of Tripod and Jacket (dimensions of structural members in mm; heights and depths in m).

Table 1 shows the frequencies of support structure modes and blades modes, in a parked state (no rotational speed) at 0° azimuth angle (one blade upward and two blade downward), for fixed and flexible FMs, the latter with force-displacement laws of the soil springs linearized to the initial tangent stiffness.

For the fixed FM, the frequencies of the first fore-aft (FA) and side-to-side (SS) support structure modes, as well as the frequencies of the blades modes, are almost the same for Tripod and Jacket, while a substantial difference exists in the second FA and SS support structure modes (FA and SS directions correspond to *x* and *y* directions in Figure 1; "yaw" and "pitch" means that the blades modes are coupled with yaw and pitch motion of the rotor [7, 18]). Shapes of first and second FA support structure modes are reported in Figure 3; those in the SS direction are similar and are not reported for brevity.

	Tripod Frequencies (Hz)		Jacket Frequencies (Hz)	
Mode description	Fixed FM	Flexible FM	Fixed FM	Flexible FM
1st Tower Side-to-Side	0.309	0.306	0.314	0.300
1st Tower Fore-Aft	0.311	0.309	0.317	0.302
1st Blade Asymetric Flapwise Yaw	0.645	0.645	0.640	0.634
1st Blade Asymetric Flapwise Pitch	0.677	0.676	0.675	0.671
1st Blade Collective Flap	0.710	0.709	0.708	0.705
1st Blade Asymetric Edgewise Pitch	1.081	1.081	1.080	1.082
1st Blade Asymetric Edgewise Yaw	1.097	1.097	1.092	1.105
2nd Blade Asymetric Flapwise Yaw	1.749	1.735	1.714	1.721
2nd Blade Asymetric Flapwise Pitch	1.848	1.863	1.937	1.924
2nd Blade Collective Flap	1.996	1.996	2.003	2.009
2nd Tower Fore-Aft	2.206	1.277	1.219	0.984
2nd Tower Side-to-Side	2.277	1.279	1.241	0.990

Table 1. Tripod and Jacket natural frequencies for fixed and flexible FMs.

As for the flexible FM, it can be observed that the frequencies of the first FA and SS support structure modes, and the frequencies of the blades modes, are practically identical to the

corresponding ones for fixed FM, while the frequencies of the second FA and SS support structure modes are decreased. All these results are in agreement with findings of similar studies [24, 27]. For design purposes, it is important to remark that the frequencies of the first FA and SS support structure modes are almost the same for Tripod and Jacket, even when foundation flexibility is accounted for. Shapes of the first and second FA and SS support structure modes are similar to those for fixed FM shown in Figure 3, and are omitted for brevity.

Stiffness and mass parameters are reported in Table 2, for fixed and flexible FMs, with non-linear laws of soil springs linearized to the initial tangent stiffness.

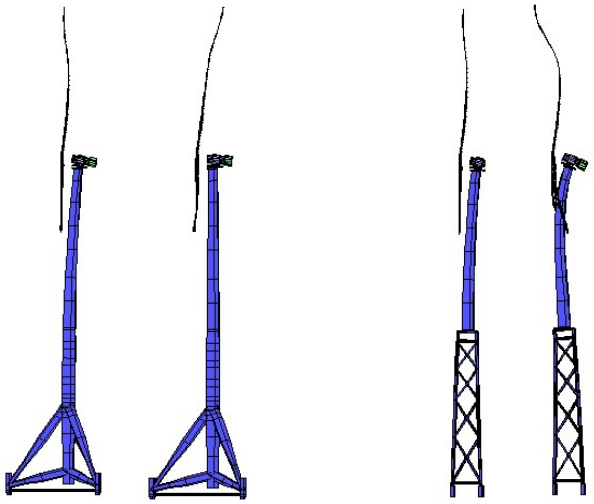

Figure 3. First and second FA support structure modes of Tripod and Jacket.

	Tripod		Jacket	
Stiffness	Fixed FM	Flexible FM	Fixed FM	Flexible FM
K_{Fx} (Nm^{-1})	$1.74 \cdot 10^6$	$1.69 \cdot 10^6$	$1.65 \cdot 10^6$	$1.58 \cdot 10^6$
K_{Fy} (Nm^{-1})	$1.74 \cdot 10^6$	$1.69 \cdot 10^6$	$1.65 \cdot 10^6$	$1.58 \cdot 10^6$
K_{Mx} (Nm)	$3.07 \cdot 10^9$	$3.07 \cdot 10^9$	$2.86 \cdot 10^9$	$2.86 \cdot 10^9$
K_{My} (Nm)	$3.07 \cdot 10^9$	$3.07 \cdot 10^9$	$2.86 \cdot 10^9$	$2.86 \cdot 10^9$
Total Mass (ton)	2844	3175	1800	2238
RNA Mass (ton)	350	350	350	350
Tower Mass (ton)	646	646	290	290

Table 2. Tripod and Jacket stiffness and mass parameters for fixed and flexible FMs.

ID No.	Year	Earthquake	Station	PGA	NEHRP class	ID No.	Year	Earthquake	Station	PGA	NEHRP class
1	1992	Cape Mendocino	P.	6.12	C	26	1989	Loma Prieta	APEEL 2	2.44	E
2	1999	Chi Chi Taiwan	TCU065	6.80	D	27	1989	Loma Prieta	F. C. – A. 1	2.75	E
3	1999	Chi Chi Taiwan	TCU102	2.17	C	28	1989	Loma Prieta	F. C. – M. C.	1.03	E
4	1999	Duzce-Turkey	D.	4.23	D	29	1989	Loma Prieta	G. A. #02	3.44	D
5	1992	Erzincan-Turkey	E.	4.43	D	30	1989	Loma Prieta	G. A. #03	4.84	D
6	1979	Imperial Valley-06	A. M.	3.06	D	31	1989	Loma Prieta	G. H. B.	2.66	D
7	1979	Imperial Valley-06	A.	2.76	D	32	1989	Loma Prieta	G. G. C.	3.42	C
8	1979	Imperial Valley-06	A. A.	1.79	D	33	1989	Loma Prieta	Larkspur	1.21	E
9	1979	Imperial Valley-06	EC C. C.	1.96	D	34	1989	Loma Prieta	S. –A.	3.62	C
10	1979	Imperial Valley-06	EC M. O.	3.11	D	35	1989	Loma Prieta	S.-W V.	3.15	C
11	1979	Imperial Valley-06	El C. A. #3	2.44	E	36	1989	Loma Prieta	T. I.	1.36	E
12	1979	Imperial Valley-06	El C. A. #4	4.04	D	37	1984	Morgan Hill	G. A. #06	2.75	C
13	1979	Imperial Valley-06	El C. A. #5	4.36	D	38	1986	North Palm Spring	N. P. S.	6.30	D
14	1979	Imperial Valley-06	El C. A. #6	4.12	D	39	1994	Northridge	J. F. P.	7.29	C
15	1979	Imperial Valley-06	El C. A. #7	3.86	D	40	1994	Northridge	N. F. S.	6.73	D
16	1979	Imperial Valley-06	El C. A. #8	5.16	D	41	1994	Northridge	N. W P. C.	3.38	D
17	1979	Imperial Valley-06	El C. A. #10	1.96	D	42	1994	Northridge	P. D. d.	3.43	A
18	1979	Imperial Valley-06	El C. A. #11	3.67	D	43	1994	Northridge	R.	5.95	D
19	1979	Imperial Valley-06	El C. D. A.	4.22	D	44	1994	Northridge	S. C. S.	6.74	D
20	1979	Imperial Valley-06	H. P. O.	2.40	D	45	1994	Northridge	S. C. E.	6.32	C
21	1979	Imperial Valley-07	El C. A. #3	1.40	E	46	1994	Northridge	S. S. O. V.	6.48	C
22	1980	Irpinia	S.	2.61	B	47	1987	Superstition Hills	P. T. S.	3.72	D
23	1995	Kobe-Japan	KJMA	6.71	D	48	1987	Superstition Hills	El C. I.	2.57	D
24	1999	Kocaeli	Ambarli	2.10	E	49	1987	Whittier Narrows	C. – W. S.	1.11	E
25	1989	Landers	L.	7.41	C						

Table 3. Earthquake set from ref. [20-21].

3. LOAD CASES

The earthquake set for seismic assessment includes 49 real records listed in Table 3, taken from ref. [20-21]. Each record has two horizontal components. Figure 4a shows the 5% damped acceleration response spectrum, computed as the maximum square root of the sum of the squares (SRSS) of the acceleration responses under the two horizontal components [10]. It can be seen that many frequencies of Tripod and Jacket, reported in Table 1, fall within the range of significant spectral accelerations (for reference, Figure 4a includes only the periods of the first and second FA support

structure modes, for fixed FM: T_1 = 1/0.311 = 3.215, T_2 = 1/2.206 = 0.453 for the Tripod; T_1 = 1/0.317 = 3.155, T_2 = 1/1.219 = 0.820 for the Jacket).

Following the approach by Prowell et al. [9-10], who have extensively studied the seismic response of a land-based NREL 5MW HAWT, seismic effects are investigated in different scenarios, considering three load cases:

LC1 = Earthquake loads and operational wind-wave loads, for a wind speed at hub height $V_{hub} = 11.4\ \mathrm{m\,s^{-1}}$, a wave period $T_p = 9.5\ \mathrm{s}$ and a significant wave height $H_s = 5.0\ \mathrm{m}$.

LC2 = Earthquake loads and emergency stop loads, for a wind speed at hub height $V_{hub} = 11.4\ \mathrm{m\,s^{-1}}$, a wave period $T_p = 9.5\ \mathrm{s}$ and a significant height $H_s = 5.0\ \mathrm{m}$. It is assumed that the emergency stop is activated as the nacelle acceleration exceeds 1 $\mathrm{ms^{-2}}$. This value is well higher than the nacelle accelerations due to the considered environmental state, and is in agreement with the emergency stop nacelle acceleration used for land-based HAWTs [9-10].

LC3 = Earthquake loads and wind-wave loads in a parked state, for a wind speed at hub height $V_{hub} = 40\ \mathrm{m\,s^{-1}}$, a wave period $T_p = 11.5\ \mathrm{s}$ and a significant wave height $H_s = 7.0\ \mathrm{m}$.

Wind and wave parameters have been chosen based on the following criteria. In load cases LC1 and LC2, $V_{hub} = 11.4\ \mathrm{m\,s^{-1}}$ is the rated wind speed of the 5MW turbine, i.e. the minimum wind speed at which the turbine generates its designated maximum power [2]; since turbines are generally designed to provide maximum power for wind speeds with high probability of occurrence at the site, $V_{hub} = 11.4\ \mathrm{m\,s^{-1}}$ can reasonably be assumed as a most likely operational wind speed. In load case LC3, $V_{hub} = 40\ \mathrm{m\,s^{-1}}$ is a very high wind speed, at which the turbine will certainly be parked, i.e. not operating. Consistently with similar studies [18], wave periods T_p and significant

heights H_s have been chosen as those associated with the selected wind speeds V_{hub} in typical offshore environmental states, as for instance some encountered in the Pacific Ocean [28].

It is assumed that wind and waves act both in *x* direction (Figure 1). Samples are generated in BLADED based on pertinent power spectra [22]. The Kaimal spectrum is used for the wind process [2, 29]:

$$S_k(f) = \frac{4\sigma_k^2 L_k / V_{hub}}{\left(1 + 6f L_k / V_{hub}\right)^{5/3}} \tag{1}$$

where f is the frequency (Hz), k is the index referring to the velocity component (1 = x direction, 2 = y direction and 3 = z direction), σ_k is the standard deviation and L_k is the integral scale parameter of each velocity component. Assuming medium turbulence characteristics [27], all parameters in Eq.(1) are set according to IEC 61400-1 prescriptions for a normal turbulence model [2]. The JONSWAP spectrum is used for the wave process [30]:

$$S_{JS}(f) = \alpha_2 H_s^2 T_p \left(\frac{f}{f_p}\right)^{-5} \exp\left[-1.25\left(\frac{f}{f_p}\right)^{-4}\right] \cdot \gamma^{\beta} \tag{2}$$

where $f_p = 1/T_p$, γ is the JONSWAP peakedness parameter [3]

$$\gamma = \begin{cases} 5 & T_p/\sqrt{H_s} \le 3.6 \\ \exp\left(5.75 - 1.15 T_p/\sqrt{H_s}\right) & 3.6 \le T_p/\sqrt{H_s} \le 5.0 \\ 1 & T_p/\sqrt{H_s} \le 5.0 \end{cases} \tag{3}$$

and

$$\alpha_2 = \frac{0.0624}{0.230 + 0.0336\gamma - \dfrac{0.185}{1.9+\gamma}} \qquad \beta = \exp\left[-\frac{0.5}{\sigma^2}\left(\frac{f}{f_p}-1\right)^2\right] \qquad \sigma = \begin{cases} 0.07 & f \le f_p \\ 0.09 & f > f_p \end{cases} \tag{4a,c}$$

The Kaimal and JONSWAP spectra for the considered environmental states are reported in Figure 4b, along with the rotor frequency band (1P) and blade passing frequency band (3P) of the 5MW HAWT [31]. It can be observed that the frequencies of the first FA support structure modes of both Tripod and Jacket fall within the interval 1P-3P, corresponding to a typical soft-stiff design.

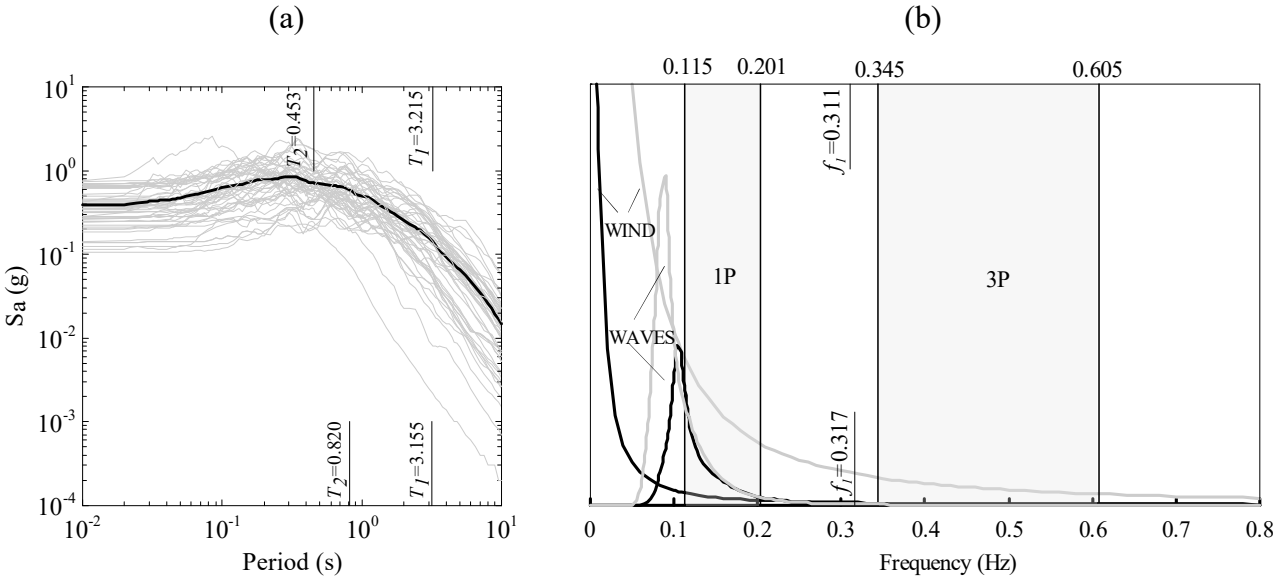

Figure 4. (a) 5% damped SRSS acceleration response spectrum for the earthquake set (black line: mean value); (b) wind and wave power spectral densities (black line: load cases LC1/LC2; grey line: load case LC3).

Fully-coupled non-linear time-domain simulations are carried out in BLADED by numerical integration of motion equations built by a combined multi-body dynamics and modal approach [22], considering interactions of aerodynamic, hydrodynamic and seismic responses, and including non-linear soil stiffness as modelled in Section 2. While the aerodynamic loading on the spinning rotor is generated based on classical concepts of combined blade element and momentum theory [32], the hydrodynamic loading on the structural members is computed based on Morison's equation [33],

with drag and inertia coefficients set according to DNV recommendations [5]. Wind loads acting along the tower are included. For both Tripod and Jacket, modal damping ratios are set equal to 10^{-2} for support structure modes, and 4.775×10^{-3} for the blades modes [13]. The simulation length is 800 sec, with the earthquake ground motion starting 400 seconds into the simulation, to ensure that the earthquake occurs as the structural response has already attained a steady state [9-10].

4. RESPONSE TO A SINGLE EARTHQUAKE RECORD

To gain a preliminary insight into the response of Tripod and Jacket under combined wind, wave and earthquake loading, the response to a single earthquake is discussed. Specifically, the Northridge earthquake is considered (ID No. 44 in Table 3), a 40 second duration near fault ground motion [21]. Results are obtained assuming that the fault normal and fault parallel components act in *x* and *y* directions, respectively (see Figure 1).

The response is computed for load cases LC1, LC2 and LC3 in Section 3. For each load case, one sample of the wind process and one sample of the wave process are generated based on the spectra given in Eq.(1) and Eq.(2). For load case LC3, 0° and 180° azimuth angles are considered for the parked rotor (180° = two blades upward and one blade downward). Tower top deflection and maxima accelerations along the support structures are given in Figures 5-6, for fixed and flexible FMs.

4.1. Response for fixed foundation model

Figures 5a-b and Figures 6a-b show the tower top deflection in *x* and *y* directions, for fixed FM. For both Tripod and Jacket, it is observed that:

(1) If the earthquake occurs in the operational state, the tower top deflection increases significantly starting from the earthquake strike (time history above t=400 sec), reducing progressively to the operational deflection once the earthquake has expired (time history above t=440 sec).

(2) As a result of an emergency stop triggered at a 1 ms^{-2} nacelle acceleration, the tower top deflection deviates from the operational deflection and, after a transient, attains a parked state, where the deflection is due only to wave loads, and wind loads acting on the parked rotor and along the tower.

(3) If the earthquake occurs in a parked state, the tower top deflection increases starting from the earthquake strike reducing progressively to the parked deflection. Differences between the 0° and 180° parked states are not noticeable. It can be argued that, although the geometry of the two rotor positions is different, the difference in terms of mass distributions along the height is relatively small, with a consequent relatively small effect on the seismic response. Notice that, once the earthquake has expired, the final parked deflections in load cases LC2 and LC3 are different, due to the fact that load case LC2 and load case LC3 involve different wind speeds V_{hub}, wave periods T_p and significant wave heights H_s.

Figure 5c and Figure 6c show the maxima accelerations along the support structures, in *x* and *y* directions. The acceleration profile in *x* direction shows that combined wind-wave-earthquake loadings activate first and second FA support structure modes, in both Tripod and Jacket, in all three load cases under investigation. The same observation can be made based on the acceleration profile in *y* direction. The activation of the second FA and SS support structure modes is confirmed by the fact that the acceleration profiles exhibit significant values at approximately 2/3 of the support structure height, and this result is consistent with analogous results for land-based HAWTs under earthquake loading [11].

TRIPOD

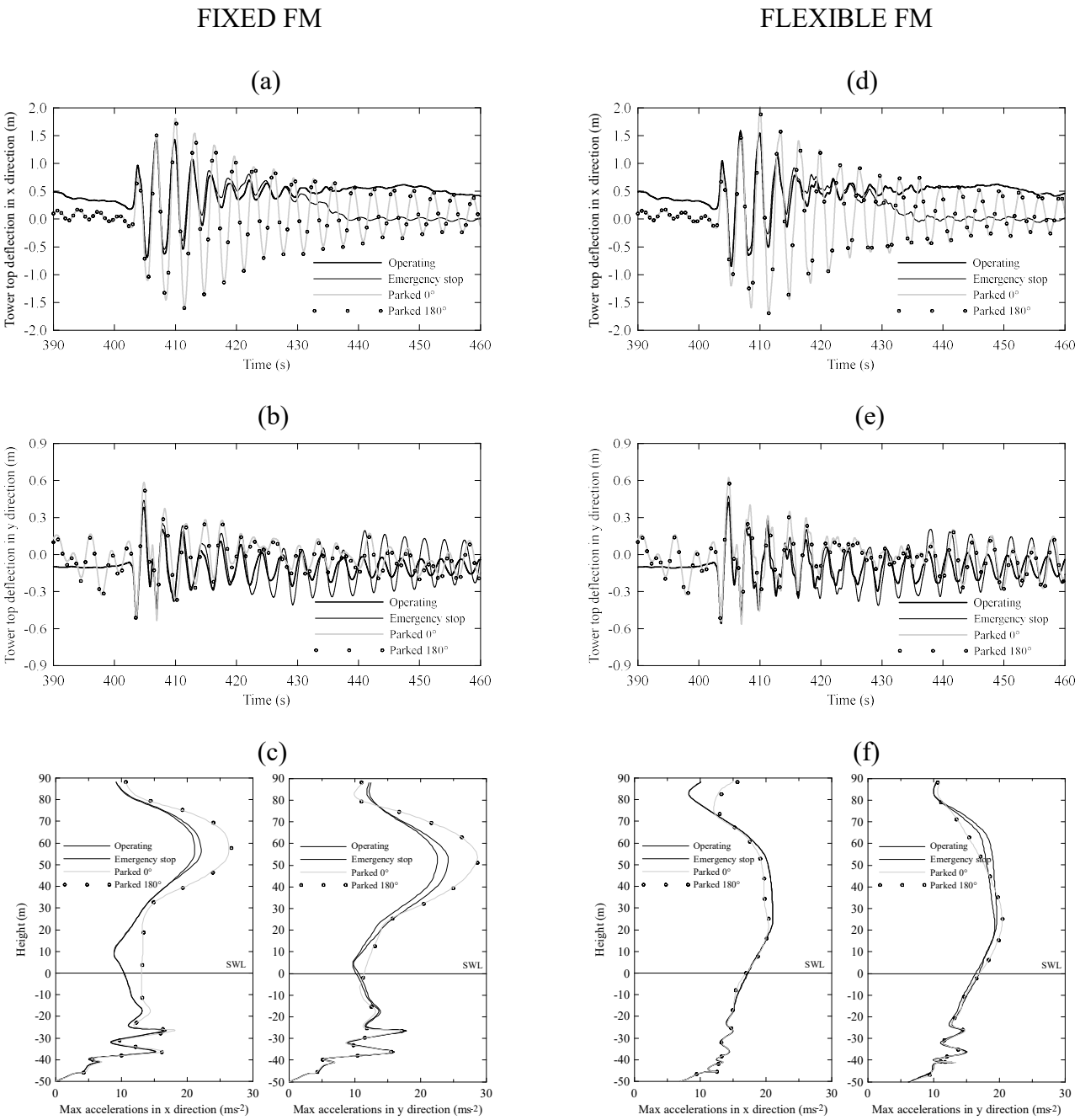

Figure 5. Tripod: tower top deflection and maxima acceleration profiles in *x* and *y* direction for fixed and flexible FMs.

JACKET

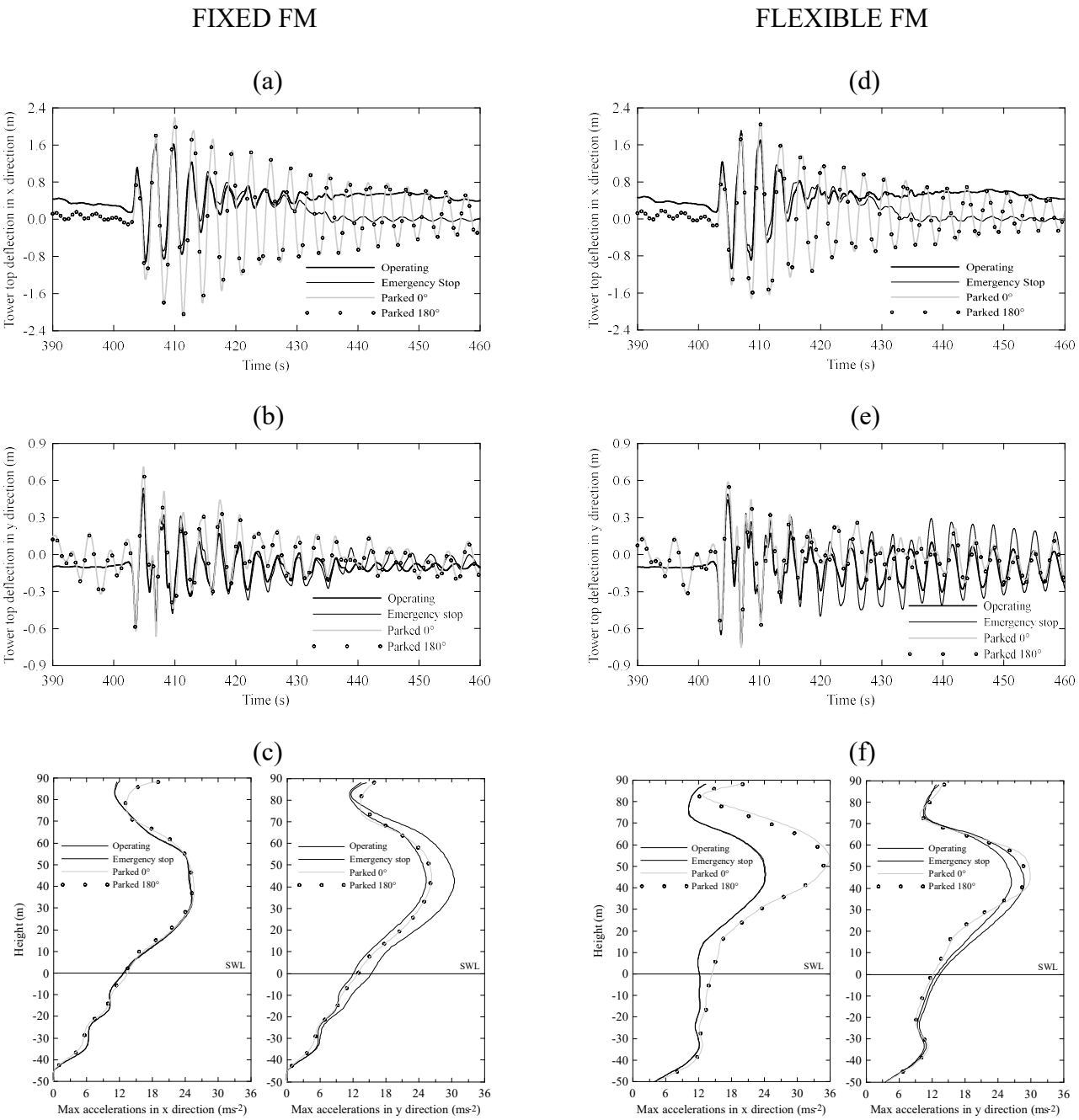

Figure 6. Jacket: tower top deflection and maxima acceleration profiles in *x* and *y* direction for fixed and flexible FMs.

4.2. Response for flexible foundation model

Figures 5d-e-f and Figures 6d-e-f show the tower top deflection and maxima accelerations along the support structures, in *x* and *y* directions, for flexible FM. Results appear in agreement with the corresponding ones for fixed FM. That is, the tower top deflection is significantly affected by the

earthquake strike, with a considerable increase with respect to the operational deflection in load case LC1, a deviation from the operational deflection and subsequent transient in load case LC2, an increase with respect to the parked deflection in load case LC3, with no noticeable differences between 0° and 180° parked states. The acceleration profiles show contributions from first and second support structure modes. Also, it is seen that deflections and accelerations of the tower top are slightly larger, in most cases, than those for fixed FM.

5. RESPONSE TO AN EARTHQUAKE SET

Next, the seismic response of Tripod and Jacket is investigated using the full earthquake set in Table 3, for load cases LC1-LC2-LC3 introduced in Section 3. In particular, considering that the results of load case LC3 do not seem affected by the rotor position, a 0° parked state is assumed. For a given load case, two simulations are carried out for each earthquake, in agreement with the studies by Prowell et al. [9-10] on land-based HAWTs. The two simulations differ as the two horizontal components of the earthquake are rotated 90 degrees, in order to reduce bias from the orientation of the earthquake components relative to the wind direction [9-10]. Therefore, each load case involves 98=49×2 simulations.

For each simulation, some results of particular interest are considered as measures of the earthquake demand: maximum resultant bending moment at the tower base (= maximum SRSS of the bending moments in x and y directions); maximum axial force at the pile head, for pile #1' of the Tripod and pile #3" of the Jacket (see Figure 1); maximum resultant bending moment at the blade root (= maximum SRSS of the bending moments in orthogonal planes of the blade local coordinate system); maximum resultant acceleration at the tower top (= maximum SRSS of the accelerations in x and y directions). It is noticed that pile #1' of the Tripod and pile #3" of the Jacket are selected since, according to the simulation results, they undergo slightly higher demands with respect to the other piles. However, variability of results is very limited and, from an engineering point of view,

demands in all piles can be considered within the same range, in all load cases LC1-LC2-LC3. For completeness, results for all piles are reported in the ESM attached to the paper.

Results are reported in Figures 7-8 assuming the peak ground acceleration (PGA) as earthquake intensity measure, for fixed and flexible FMs. In total, 588=2×3×98 simulations have been run for each structure.

5.1. Stress resultant and tower top acceleration demands for fixed foundation model

In Figures 7-8, stress resultant and tower top acceleration demands for fixed FM are denoted by symbol "×". Black vertical lines indicate the corresponding demands due to wind and wave loads only, i.e. without earthquake loads, for the environmental states considered in load cases LC1-LC2-LC3 (see Section 3).

Firstly, some relevant comments are in order on the stress resultant demands at the tower base and pile head. For both Tripod and Jacket it can be seen that, as a result of the earthquake strike, stress resultant demands increase significantly, in all load cases LC1-LC2-LC3. In particular, considering that in both Tripod and Jacket the maxima stress resultant demands without earthquake loads are attained in the operational state (black vertical lines in load case LC1 of Figures 7-8), maxima stress resultant demands due to earthquake loads increase by a factor of 2-3 at the tower base and by a factor of 8-9 at the pile head of the Tripod (Figure 7), by a factor of 3-4 at the tower base and by a factor of 4-5 at the pile head of the Jacket (Figure 8). Further important observations are that significant stress resultant demands are encountered not only for high, but also for moderate PGA, and that stress resultant demands in load cases LC1-LC2-LC3 can be considered to be practically within the same range (100-400 MNm at the tower base and 10-80 MN at the pile head of the Tripod; 50-400 MNm at the tower base and 15-80 MN at the pile head of the Jacket). In this regard, it is worth noticing that stress resultant demands in the parked state (load case LC3) falling within the same range of stress resultant demands in the operational state (load case LC1) have been observed also in the seismic response of land-based HAWTs [8-10]. This result can be explained

considering that, when the turbine is parked, the only damping is the structural damping of the support structure, usually low in steel structures, while in the operational state the structural response experiences an additional aerodynamic damping, whose source is essentially the spinning rotor aerodynamics, and that depends on the oscillations of the tower top due to earthquake loading [34-35]. It is also worth noticing that the significant stress resultant demands found in case of an emergency stop (load case LC2), shown in Figures 7-8, mean that triggering a shutdown does not provide substantial benefits and that, therefore, load case LC2 shall generally be considered in the seismic assessment. In this context, it is pointed out that in all simulations of load case LC2 earthquake loads do trigger an emergency stop, i.e. the nacelle acceleration exceeds 1 ms^{-2}.

Comments on stress resultant demands at the tower base and pile head hold also for the tower top accelerations. Figures 7-8 show indeed that the tower top acceleration demands are significantly higher than the corresponding values without earthquake loads, in all load cases LC1-LC2-LC3.

As for the moment demands at the blade root, Figures 7-8 show that in both Tripod and Jacket they are not affected by an earthquake strike in the operational state (load case LC1) and in case of an emergency stop (load case LC2), while increments are experienced in the parked state (load case LC3); considering that the maxima moment demands without earthquake loads are attained in the operational state (black vertical lines in load case LC1), maxima moment demands increase by a factor of 1.2 in the Tripod (Figure 7), and by a factor of 2 in the Jacket (Figure 8). This result is evidence that seismic-induced blade vibrations are damped by aerodynamic damping in the operational state, but become significant in the parked state due to very low structural damping of the blades, in agreement with similar findings for land-based HAWTs [10]. For completeness, a comment is in order on symbols "×" on the left of the vertical lines in load case LC2, that correspond to simulations in which the maximum blade root bending moment after the start of earthquake shaking is found to be smaller than the maximum due to the considered operational wind-wave loads. This may happen considering that: (i) on one hand, the emergency stop may be activated just a few seconds after the start of earthquake shaking, i.e. when not enough time has

elapsed for earthquake loads to cause moments higher than the maximum moment due to the operational wind-wave loads; (ii) on the other hand, after the activation of the emergency stop the moments caused by the combined earthquake loads + emergency stop loads may not exceed the maximum moment due to the operational wind-wave loads. However, there are also simulations in load case LC2 (symbols "×" on the right of the vertical lines) in which after the start of earthquake shaking, either before or after the activation of the emergency stop, the maximum moment slightly exceeds the maximum due to the operational wind-wave loads, especially for high PGAs.

Comparing the responses of Tripod and Jacket, it is worth recalling that the frequencies of the first FA and SS support structure modes, as well as the frequencies of the blades modes (Table 1), are almost identical for the two structures; stress resultant demands at the tower base and pile head are found approximately within the same range, but moment demands at the blade root are generally higher in the Jacket, with a maximum demand nearly equal to 40 MNm (Figure 8) vs. 20 MNm in the Tripod (Figure 7). It is evident that these differences shall be attributed to dissimilar stiffness and mass distributions along the two support structures (Table 2) and, also, to the activation of the second FA and SS support structure modes, whose frequencies are substantially different in the Tripod and Jacket (Table 1).

A final important comment is that, as shown in Figures 7-8, stress resultant and tower top acceleration demands generally increase with the PGA, thus meaning that the PGA can be taken as an acceptable indicator of demand for the structures under study. Because the PGA is typically related to the short period energy content of the earthquake, this result reflects the fact that the rotor modes and second support structure modes (Table 1) play an important role in the seismic response, as shown in Figure 4a (periods of the rotor modes and second support structure modes fall in the region of maxima spectral accelerations) and Figures 5-6 (activation of the second support structure modes), in agreement with similar findings for land-based HAWTs [8-10].

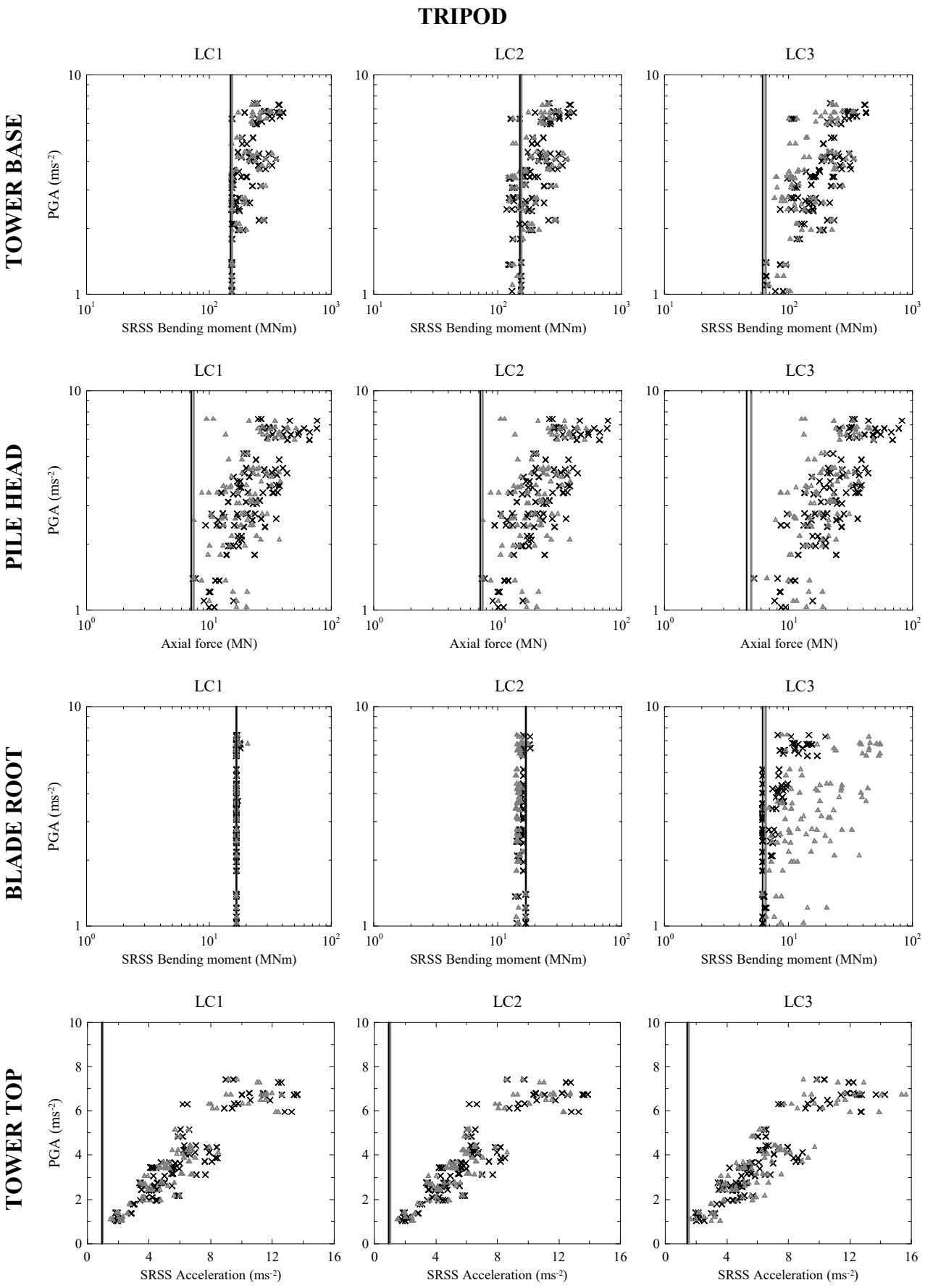

Figure 7. Tripod: stress resultant and tower top acceleration demands under the earthquake set for fixed and flexible FMs.

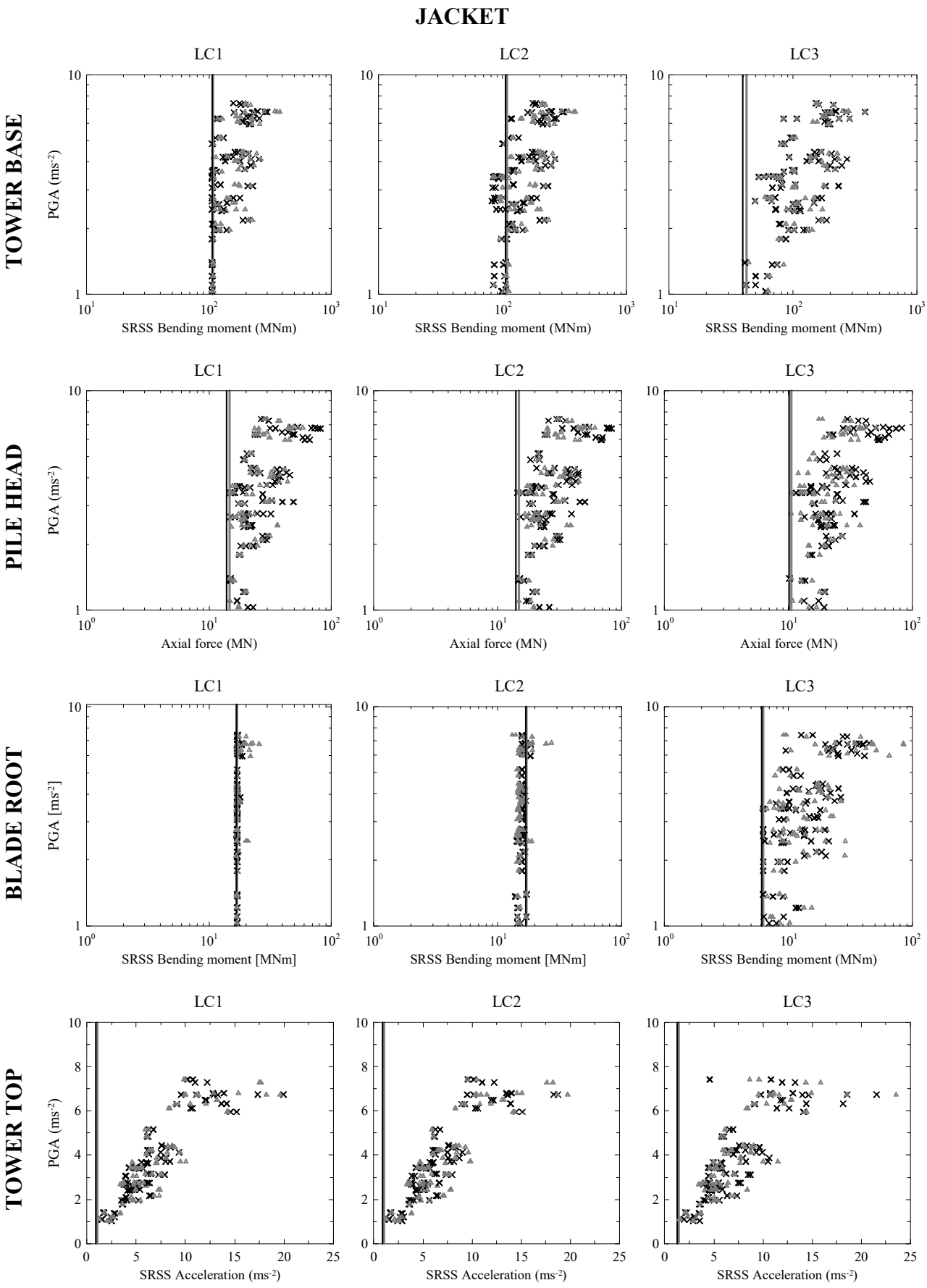

Figure 8. Jacket: stress resultant and tower top acceleration demands under the earthquake set for fixed and flexible FMs.

5.2. Stress resultant and tower top acceleration demands for flexible foundation model

In Figures 7-8, stress resultant and tower top acceleration demands for flexible FM are denoted by symbol "Δ", while grey vertical lines indicate the corresponding demands due to wind and wave loads only, for the environmental states in load cases LC1-LC2-LC3 (see Section 3).

At the tower base and pile head, in both Tripod and Jacket, stress resultant demands do not change significantly with respect to the corresponding demands for fixed FM, in all load cases LC1-LC2-LC3. This result may be explained considering that the frequencies of the first FA and SS support structure modes, as well as the frequencies of the blades modes, hold almost the same values for fixed and flexible FMs (Table 1), while the frequencies of second FA and SS support structure modes, although being reduced by the foundation flexibility (Table 1), still correspond to periods falling within the range of high spectral accelerations, as shown in Figure 4a (for instance, for the second FA support structure modes: $T_2 = 1/1.277 = 0.783$ s in the Tripod, and $T_2 = 1/0.984 = 1.016$ s in the Jacket). The same observations can be made for the stress resultant demands at the tower base and pile head without earthquake loads (grey vertical lines in load cases LC1-LC2-LC3), which appear almost identical to the corresponding demands for fixed FM (black vertical lines), showing that frequencies of the second FA and SS support structure modes, although being reduced by the foundation flexibility, shift within a frequency range that is still relatively far from the excitation frequencies of wind and wave processes (Figure 4b).

Figures 7-8 also show that, unlike the stress resultant demands at the tower base and pile head, moment demands at the blade root in the parked state (load case LC3) increase with respect to the corresponding demands for fixed FM, in both Tripod and Jacket. In particular, the maximum moment demand in the Tripod is found to be 60 MNm (vs. 20 MNm for fixed FM), while that in the Jacket is 90 MNm (vs. 40 MNm for fixed FM). It is interesting to remark that, as shown in Figures 7-8, such an increase of maximum moment demand at the blade root mirrors an increase of maximum tower top acceleration in the parked state (load case LC3) with respect to the

corresponding maximum acceleration for fixed FM, and shall be considered, in this case, as a result of the additional flexibility introduced by the flexible FM [36].

Comparing Tripod and Jacket responses, it is observed that stress resultant demands at the tower base and pile head fall approximately within the same range, while the maximum moment demand at the blade root is encountered in the Jacket (90 MNm). In these respects, results appear in a substantial agreement with those for fixed FM.

TRIPOD **JACKET**

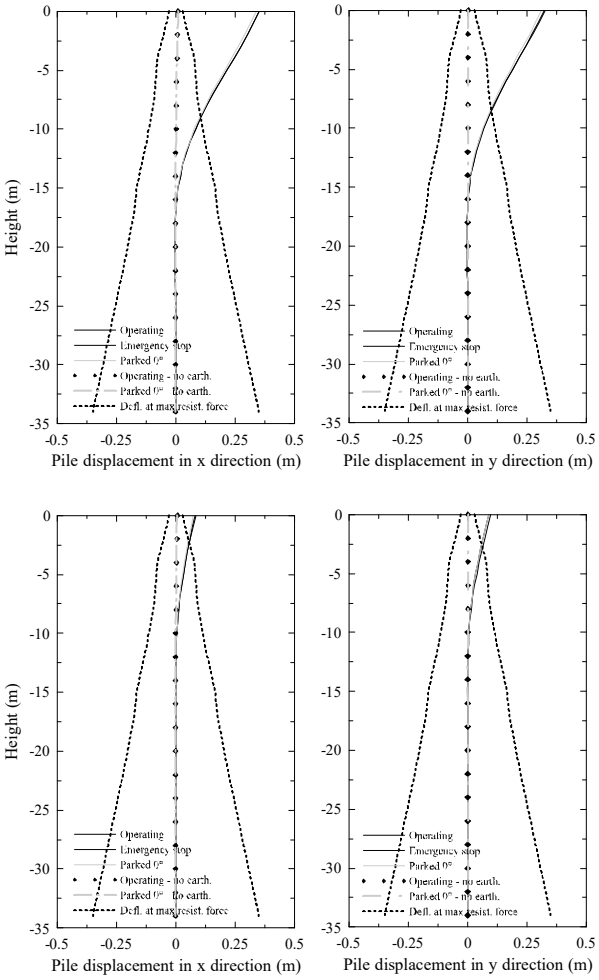

Figure 9. Tripod and Jacket pile maxima lateral deflections in *x* and *y* directions.

In order to have an indicator of non-linearity of the soil response, the maxima lateral *x*- and *y*-deflections obtained from all simulations of the earthquake set, at various depths along the piles, are reported in Figure 9 for load cases LC1-LC2-LC3. Here, the maximum deflection has to be

intended as the maximum deviation from the initial vertical configuration of the pile and, as such, may be found in either the positive or negative direction of x and y axes. In particular, it has been found that the maxima lateral deflections at all depths are attained in the same simulation, and at the same time instant of the simulation, specifically as the pile head attains its maximum deflection. For example, in pile #1' of the Tripod, the maxima x-deflections at all depths are found in the simulation with the Northridge earthquake (ID No. 43 in Table 3), when its fault normal component acts in x direction. It is observed that the profiles in Figure 9, with positive and negative deflections (the latter are slightly visible, for instance, in pile #1' of the Tripod), are in accordance with typical deflection profiles of flexible piles constrained by lateral springs, supporting structures under dynamic lateral loads [37]. For comparison, Figure 9 includes also: (i) the maxima lateral deflections due to wind-wave loads only (no earthquake loads), for the environmental states considered in load cases LC1-LC2-LC3; (ii) the lateral deflections at which the soil resistance forces attain, with a tolerance of 10^{-2}, the maxima asymptotic values given by the p-y API curves [26] for the considered sandy soil [18-19], at various depths along the piles; notice that these lateral deflections can be taken as indicators of a significant non-linear soil response, because p-y curves deviate from linearity also for relatively small soil displacements [26]. Figure 9 shows that earthquake loads cause a considerable increase of lateral deflections with respect to corresponding values without earthquake loads. It is also seen that non-linear effects are significant, especially in the Tripod, where maxima lateral deflections are well above the lateral deflections corresponding to maxima soil resistance forces, over about one fourth of the total pile length. These results suggest that using linearized p-y curves, as for instance in simplified fatigue analysis of offshore HAWTs on bottom-fixed support structures [38], may not be appropriate for seismic assessment. For several motions of the earthquake set, the lateral deflection profiles at the maximum deflection of the pile head have been included as Electronic Supplementary Material (ESM) attached to the paper, in order to show that non-linear effects in the soil response are generally significant, although to a lesser extent than in Figure 9.

6. COMPARISON WITH IEC 61400-3 LOAD CASES

In order to assess whether earthquake loads are design driving for the Tripod and Jacket under study, a full set of design load cases should be considered, as for instance those prescribed by IEC 61400-3 [3]. Analyses should be carried out for site-specific conditions, based on accurate joint statistics of wind and wave states, sea currents and water level, and on a proper description of local seismicity, as required by IEC 61400-3 [3].

Here it is of interest to compare the earthquake demands in Figures 7-8, obtained for earthquake loads combined with wind-wave loads in a typical operational state and a typical parked state, with demands from some IEC 61400-3 design load cases [3]. For this purpose, the load cases in Table 4 are selected as representative of operational and parked states [3], assuming environmental parameters that can reasonably be expected in offshore sites for wind turbines, in accordance with those in Section 3 (more details on the environmental parameters in Table 4 are reported in the ESM attached to the paper). Bearing in mind that a definitive answer as to whether earthquake loads are design driving can be given only for site-specific conditions, that the environmental parameters in Table 4 may not reflect particularly unfavourable site conditions, and that only a few environmental states are selected in Table 4 (e.g., DLC 1.3 and DLC 1.6 would require discrete values of the wind speed at the hub, V_{hub}, ranging from the cut-in speed V_{in} =3.0 ms^{-1} and the cut-out speed V_{out}=25 ms^{-1} of the 5MW turbine [13] with intervals of 2 ms^{-1} [3]), it is believed that the load cases in Table 4 can provide at least a reasonable order of magnitude of typical operational and parked state demands as prescribed by IEC 61400-3 [3], for comparison with the earthquake demands in Figures 7-8.

For each load case, six simulations are implemented in BLADED [22], with either 10 min or 1-hour length [3]. Maxima stress resultants at the tower base, pile head (pile #1' of the Tripod, pile #3" of the Jacket) and blade root are reported in Tables 5-6. Maxima axial forces in the other piles

are found within the range of those in Tables 5-6 and, for completeness, are reported as ESM attached to the paper.

Hence, according to IEC 61400-3 [3], the demands in Tables 5-6 should be multiplied by a load safety factor equal to 1.35 and, for the operational load cases involving a wind speed range (Section 7.5.4 in ref. [3]), a second multiplicative factor should be considered to extrapolate appropriate long-term characteristic demands, based on a site-specific joint probability distribution of wind and wave states. Although different approaches exist to compute such extrapolation factor, indicative values of 1.2÷1.3 may be derived from land-based HAWTs (see ref. [9-10] or Annex F in ref. [2] for the characteristic moment at the blade root). Therefore, multiplying the values in Tables 5-6 by a 1.35 load safety factor and also by a 1.3 extrapolation factor for the operational load cases, it can readily be observed that the derived demands would be smaller than the earthquake demands obtained for the highest levels of PGA, as reported in Figures 7-8. It is also worth noticing that, at the pile head and blade root of the Tripod, earthquake demands would be higher also for moderate levels of PGA. In particular, at the blade root this holds true for the flexible FM (see Figure 7).

Operational state	Wind	Waves	Sea currents	Water level
DLC 1.3_1	V_{hub}=10 ms^{-1}	H_s= 5.0 m T_p= 9.53 s	$U_w(0)$=0.069 ms^{-1}	MSL=50 m
DLC 1.3_2	V_{hub}=15 ms^{-1}	H_s= 5.5 m T_p= 10.0 s	$U_w(0)$=0.105 ms^{-1}	MSL=50 m
DLC 1.3_3	V_{hub}=20 ms^{-1}	H_s= 6.0 m T_p= 10.4 s	$U_w(0)$=0.139 ms^{-1}	MSL=50 m
DLC 1.3_4	V_{hub}=25 ms^{-1}	H_s= 6.5 m T_p= 10.9 s	$U_w(0)$=0.174 ms^{-1}	MSL=50 m
DLC 1.6a_1	V_{hub}=10 ms^{-1}	H_s=8.0 m T_p=12 s	$U_w(0)$=0.069 ms^{-1}	NWLR=52 m
DLC 1.6a_2	V_{hub}=15 ms^{-1}	H_s=8.0 m T_p=12 s	$U_w(0)$=0.105 ms^{-1}	NWLR=52 m
DLC 1.6a_3	V_{hub}=20 ms^{-1}	H_s=8.0 m T_p=12 s	$U_w(0)$=0.139 ms^{-1}	NWLR=52 m
DLC 1.6a_4	V_{hub}=25 ms^{-1}	H_s=8.0 m T_p=12 s	$U_w(0)$=0.174 ms^{-1}	NWLR=52 m
DLC 1.6a_5	V_{hub} =10 ms^{-1}	H_s=8.0 m T_p=12 s	$U_w(0)$=0.069 ms^{-1}	NWLR=48 m
DLC 1.6a_6	V_{hub}=15 ms^{-1}	H_s=8.0 m T_p=12 s	$U_w(0)$=0.105 ms^{-1}	NWLR=48 m
DLC 1.6a_7	V_{hub}=20 ms^{-1}	H_s=8.0 m T_p=12 s	$U_w(0)$=0.139 ms^{-1}	NWLR=48 m
DLC 1.6a_8	V_{hub}=25 ms^{-1}	H_s=8.0 m T_p=12 s	$U_w(0)$=0.174 ms^{-1}	NWLR=48 m

Parked state	Wind	Waves	Wave dir.	Sea currents	Water level
DLC 6.1a_1	V_{hub}=47.5 ms^{-1}	H_s=8.7 m T_p=12.6 s	+30°	$U_w(0)$=0.37 ms^{-1} $U_{ss}(0)$=3.0 ms^{-1}	EWLR=53 m
DLC 6.1a_2	V_{hub}=47.5 ms^{-1}	H_s=8.7 m T_p=12.6 s	0°	$U_w(0)$=0.37 ms^{-1} $U_{ss}(0)$=3.0 ms^{-1}	EWLR=53 m
DLC 6.1a_3	V_{hub}=47.5 ms^{-1}	H_s=8.7 m T_p=12.6 s	–30°	$U_w(0)$=0.37 ms^{-1} $U_{ss}(0)$=3.0 ms^{-1}	EWLR=53 m
DLC 6.1a_4	V_{hub}=47.5 ms^{-1}	H_s=8.7 m T_p=12.6 s	+30°	$U_w(0)$=0.37 ms^{-1} $U_{ss}(0)$=3.0 ms^{-1}	EWLR=47 m
DLC 6.1a_5	V_{hub} =47.5 ms^{-1}	H_s=8.7 m T_p=12.6 s	0°	$U_w(0)$=0.37 ms^{-1} $U_{ss}(0)$=3.0 ms^{-1}	EWLR=47 m

DLC 6.1a_6	V_{hub}=47.5 ms^{-1}	H_s=8.7 m T_p=12.6 s	–30°	$U_w(0)$=0.37 ms^{-1}	$U_{ss}(0)$=3.0 ms^{-1}	EWLR=47 m

Table 4. IEC 61400-3 load cases [3], for comparison with earthquake load cases LC1-LC2-LC3.

Although the considered operational and parked states are certainly not exhaustive, and other important loads shall be considered in design analyses, such as fatigue loads, the results discussed above substantiate the need for an accurate seismic assessment of offshore HAWTs, also in recognition of the fact that no load safety factor has been applied to earthquake demands when compared to the demands from the IEC 61400-3 load cases. Analogous conclusions have been drawn in studies on a land-based NREL 5MW HAWT [9-10], showing that earthquake demands may be design driving in regions of high seismic hazard.

TRIPOD

Operational state	**Tower base moment (MNm)**		**Pile #1′ head axial force (MN)**		**Blade root moment (MNm)**	
	Fixed FM	Flex. FM	Fixed FM	Flex. FM	Fixed FM	Flex. FM
DLC 1.3_1	122.72	120.80	6.85	7.63	17.57	16.59
DLC 1.3_2	111.62	101.49	7.04	7.66	14.34	15.42
DLC 1.3_3	110.42	110.19	7.10	7.68	15.22	15.26
DLC 1.3_4	118.00	112.62	7.20	8.32	15.01	15.18
DLC 1.6a_1	166.02	169.14	10.72	12.06	18.82	18.78
DLC 1.6a_2	130.46	136.66	7.38	7.90	16.34	16.72
DLC 1.6a_3	110.72	108.13	9.52	9.73	14.58	14.67
DLC 1.6a_4	116.29	114.43	9.97	9.02	13.86	13.98
DLC 1.6a_5	156.11	157.18	10.30	11.73	19.04	18.78
DLC 1.6a_6	125.46	132.96	7.79	7.58	16.66	16.86
DLC 1.6a_7	104.72	103.71	9.34	9.09	14.30	14.34
DLC 1.6a_8	115.74	110.98	9.66	8.80	13.78	13.74
Parked state	**Tower base moment (MNm)**		**Pile #1′ head axial force (MN)**		**Blade root moment (MNm)**	
	Fixed FM	Flex. FM	Fixed FM	Flex. FM	Fixed FM	Flex. FM
DLC 6.1a_1	184.06	182.57	9.06	10.32	16.72	16.60
DLC 6.1a_2	185.00	183.78	10.05	11.51	16.73	16.63
DLC 6.1a_3	186.20	185.54	9.06	10.35	16.76	16.66
DLC 6.1a_4	185.51	183.20	8.01	9.86	16.69	16.62
DLC 6.1a_5	185.79	183.69	8.96	10.65	16.69	16.65
DLC 6.1a_6	186.41	184.62	7.99	9.83	16.70	16.66

Table 5. Tripod: stress resultant demands from IEC 61400-3 load cases [3] in Table 4.

JACKET

Operational state	Tower base moment (MNm)		Pile #3″ head axial force (MN)		Blade root moment (MNm)	
	Fixed FM	Flex. FM	Fixed FM	Flex. FM	Fixed FM	Flex. FM
DLC 1.3_1	69.92	68.58	16.10	15.96	16.12	15.86
DLC 1.3_2	73.53	71.49	16.97	16.52	14.47	14.69
DLC 1.3_3	72.00	74.24	17.31	16.86	15.74	15.71
DLC 1.3_4	80.24	76.30	18.24	17.49	16.54	16.39
DLC 1.6a_1	111.64	113.19	20.01	20.57	20.49	20.03
DLC 1.6a_2	86.87	82.52	16.34	16.61	17.36	16.22
DLC 1.6a_3	73.36	68.41	17.83	17.73	15.57	15.08
DLC 1.6a_4	79.12	77.38	18.56	18.16	15.66	15.74
DLC 1.6a_5	110.26	112.78	20.03	20.23	20.32	20.18
DLC 1.6a_6	82.88	74.97	15.98	16.46	16.80	16.41
DLC 1.6a_7	74.72	69.90	17.70	17.26	15.05	14.99
DLC 1.6a_8	79.48	79.44	18.21	17.95	15.44	15.64
Parked state	**Tower base moment (MNm)**		**Pile #3″ head axial force (MN)**		**Blade root moment (MNm)**	
	Fixed FM	Flex. FM	Fixed FM	Flex. FM	Fixed FM	Flex. FM
DLC 6.1a_1	123.65	122.63	30.27	25.34	16.81	16.46
DLC 6.1a_2	123.98	123.14	25.49	23.18	16.81	16.42
DLC 6.1a_3	124.11	124.26	21.06	22.25	16.83	16.38
DLC 6.1a_4	123.41	122.33	28.04	24.39	16.81	16.41
DLC 6.1a_5	123.56	122.96	23.86	22.68	16.80	16.38
DLC 6.1a_6	123.54	124.04	21.21	22.27	16.81	16.37

Table 6. Jacket stress resultant demands from IEC 61400-3 load cases in Table 4.

7. CONCLUDING REMARKS

The seismic behaviour of the NREL 5MW HAWT [13], mounted on a Tripod and a Jacket in transitional water depths, has been investigated by fully-coupled non-linear time-domain simulations on full system models implemented in BLADED [22], for fixed and flexible FMs. Some typical scenarios, i.e. earthquake striking in the operational state (load case LC1) or parked state (load case LC3), and earthquake triggering an emergency stop (load case LC2) have been considered, selecting two typical wind-wave states for operational and parked states. The main results can be summarized as follows.

(i) For the fixed FM, in both Tripod and Jacket, moment demand at the tower base and axial force at the pile head in load cases LC1-LC2-LC3, as well as moment demand at the blade root in load case LC3, increase significantly with respect to the corresponding demands without earthquake loads, even for moderate PGA.

(ii) For the flexible FM, in both Tripod and Jacket, moment demand at the tower base and axial force demand at the pile head do not change significantly with respect to the corresponding demands for fixed FM, while maxima moment demands at the blade root increase significantly. This is consistent with the fact that, as a result of the foundation flexibility, maxima tower top accelerations increase with respect to corresponding maxima for fixed FM [35], while, in contrast, the natural frequencies are not significantly reduced.

(iii) For both fixed and flexible FMs, demands at the tower base and pile head of both Tripod and Jacket fall approximately within the same range, while maxima moment demands at the blade root are always encountered in the Jacket. These results are evidence that different mass and stiffness distributions, as well as activation of second FA and SS support structure modes, play a crucial role in the seismic response of the two structures.

The results of load cases LC1-LC2-LC3 suggest that fully-coupled non-linear time-domain simulations on full system models, i.e. including support structure, rotor blades and nacelle, as those implementable in BLADED [22] or similar software, are highly recommended for the seismic

assessment of offshore HAWTs, while simplified models allowed by standards and guidelines [3,6], that involve only the support structure and a lumped mass modelling the RNA at the tower top, would fail to capture relevant data. These conclusions can be drawn especially considering that simplified models could not provide any prediction on the response of the rotor blades, while the simulations run in the present study have revealed that, at the blade root, moment demands are significantly increased by earthquake loads, with maxima very sensitive to foundation flexibility, and that relevant differences may exist between maxima moment demands when different support structures are used, such as the Tripod and Jacket in Figure 2. Because rotor blades are key components of the turbine, all these data are of crucial importance in the seismic assessment of offshore HAWTs. It is also recommended that full system models account for non-linear soil response, in recognition of the significant non-linear effects shown in Figure 9.

Further, the present study has shown that the stress resultant demands in load cases LC1-LC2-LC3 may be higher than demands from some typical design loads prescribed by IEC 61400-3 [3], in general for the highest levels of PGA. Although a definitive answer as to whether earthquake loads are design driving for the two structures under study can be given only considering site-specific conditions, these results substantiate the need for an accurate seismic assessment when installing offshore HAWTs in seismically active areas. In this context, refined seismic analyses should be carried out, considering vertical ground motion, variation of earthquake acceleration through soil layers [15], potential misalignment between wind and wave loads during earthquake shaking, and other important issues such as sensitivity to different models of *p-y* curves [37] and potential uncertainties in soil properties [39], alterations of the foundation stiffness due to strain-hardening or strain-softening soil behaviour [40-41]. Related effects shall be accurately investigated considering site-specific conditions.

8. REFERENCES

[1] Swan S, Hadjian AH. 1988 The 1986 North Palm Springs earthquake: Effects on power facilities. NP-5607 Research Project 2848, Electric Power Research Institute (EPRI), Palo Alto, CA.

[2] IEC 2005 *Wind turbines. Part 1: Design requirements*. IEC 61400-1 (Ed. 3). International Electrotechnical Commission, Geneva.

[3] IEC 2009 *Wind turbines. Part 3: Design requirements for offshore wind turbines*. IEC 61400-3 (Ed. 1). International Electrotechnical Commission, Geneva.

[4] GL 2012 *Guideline for the certification of offshore wind turbines*. Germanischer Lloyd, Hamburg.

[5] DNV 2013 Design of Offshore Wind Turbine Structures. DNV-OS-J101. Det Norske Veritas Copenhagen.

[6] Zhao X, Maißer P. 2006 Seismic response analysis of wind turbine towers including soil-structure interaction. *Proc. Inst. Mech. Eng., Part K: J. Multi-body Dyn.* **220**(1), 53-61. (doi: 10.1243/146441905X73691)

[7] Zhao X, Maißer P, Wu, J. 2007 A new multibody modelling methodology for wind turbine structures using a cardanic joint beam element. *Renew. Energy* **32**, 532-546. (doi:10.1016/j.renene.2006.04.010)

[8] Prowell I, Veletzos M, Elgamal A, Restrepo J. 2009 Experimental and numerical seismic response of a 65kW wind turbine. *J. Earth. Eng.* **13**(8), 1172-1190. (doi: 10.1080/13632460902898324)

[9] Prowell I, Elgamal A, Uang C, Jonkman J. 2010 Estimation of seismic load demand for a wind turbine in the time domain. In *Proc. Eur. Wind Energy Conf. Exhib.* (EWEC), Warsaw, 20-23 April.

[10] Prowell I. 2011 *An experimental and numerical study of wind turbine seismic behaviour*. PhD thesis, University of California, San Diego. (https://escholarship.org/uc/item/82b829mg)

[11] Prowell I, Elgamal A, Uang C, Luco JE, Romanowitz H, Duggan E. 2013 Shake table testing and numerical simulation of a utility-scale wind turbine including operational effects. *Wind Energy*, in press. (doi: 10.1002/we.1615)

[12] Stamatopoulos G. 2013 Response of a wind turbine subjected to near-fault excitation and comparison with the Greek Aseismic Code provisions. *Soil Dyn. Earth. Eng.* **46**, 77-84. (doi: 10.1016/j.soildyn.2012.12.014)

[13] Jonkman J, Butterfield S, Musial W, Scott G. 2009 Definition of a 5-MW reference wind turbine for offshore system development. Report No. NREL/TP-500-38060, National Renewable Energy Laboratory, Golden, CO. (http://www.nrel.gov/wind/pdfs/38060.pdf)

[14] Haciefendioğlu K. 2012 Stochastic seismic response analysis of offshore wind turbine including fluid-structure-soil-interaction. *Struct. Design Tall Spec. Build.* **21**, 867-878. (doi: 10.1002/tal.646)

[15] Kim DH, Lee SG, Lee IK. 2014 Seismic fragility analysis of 5 MW offshore wind turbine. *Renew. Energy* **65**, 250-256. (doi: 10.1016/j.renene.2013.09.023)

[16] Schwartz M, Heimiller D, Haymes S, Musial W. 2010 Assessment of offshore wind energy resources for the United States. Report No. NREL/TP-500-45889, National Renewable Energy Laboratory, Golden, CO. (http://www.nrel.gov/docs/fy10osti/45889.pdf)

[17] USGS 2008 Hazard map (PGA, 2% in 50 years). U.S. Geological Survey. (http://earthquake.usgs.gov/hazards/products)

[18] Jonkman J., Musial W. 2010 Offshore Code Comparison Collaboration (OC3) for IEA Task 23 Offshore Wind Technology and Deployment. Report No. NREL/TP-5000-48191, National Renewable Energy Laboratory, Golden, CO. (http://www.nrel.gov/docs/fy11osti/48191.pdf)

[19] Rendon EA, Manuel L. 2012 Long-term loads for a monopile-supported offshore wind turbine. *Wind Energy*. (doi: 10.1002/we.1569)

[20] ATC 2009 *Quantification of building seismic performance factors*. Report No. FEMA-P695, Applied Technology Council, Redwood City, CA. (http://www.fema.gov/media-library-data/20130726-1716-25045-9655/fema_p695.pdf)

[21] Luco N. 2001 Probabilistic seismic demand analysis, smrf connection fractures, and near source effects. PhD thesis, Stanford University. (http://geohazards.cr.usgs.gov/staffweb/nluco/manuscripts/0206--Luco.pdf)

[22] Bossanyi EA. 2000 Bladed for Windows User Manual. Garrad Hassan and Partners, Bristol.

[23] Vorpahl F, Popko W, Kaufer D. 2013 Description of a Basic Model of the 'UpWind Reference Jacket' for Code Comparison in the OC4 Project under IEA Wind Annex 30. Technical report, Fraunhofer Institute for Wind Energy and Energy System Technology IWES, Bremerhaven, Germany.(http://www.iwes.fraunhofer.de/content/dam/iwes/en/documents/OC4%20Jacket%20Model%20Description.pdf)

[24] Zaaijer MB. 2006 Foundation modelling to assess dynamic behaviour of offshore wind turbines. *Applied Ocean Research* **28**, 45-57. (doi:10.1016/j.apor.2006.03.004)

[25] AlHamaydeh M, Hussain S. 2011 Optimized frequency-based foundation design for wind turbine towers utilizing soil–structure interaction. *Journal of the Franklin Institute* **348**(7): 1470-1487. (doi: 10.1016/j.jfranklin.2010.04.013)

[26] API 2000 *Recommended practice for planning, designing and constructing fixed offshore platforms – Working stress design*. API RP 2A-WSD (21st Ed.). American Petroleum Institute. Washington, DC.

[27] Dong W, Moan T, Gao Z. 2011 Long-term fatigue analysis of multi-planar tubular joints for jacket-type offshore wind turbine in time domain. *Eng. Struct.* **33**, 2002-2014. (doi:10.1016/j.engstruct.2011.02.037)

[28] Marine Innovation & Technology 2009 ClubStead Preliminary Analysis: Metocean Conditions. Report No. MI&T040-08_R2. Marine Innovation & Technology, Berkeley, CA. (http://www.seasteading.org/wp-content/uploads/2013/03/ClubStead-Metoceanv0a.pdf)

[29] ABS 2011 *Design Standards for Offshore Wind Farms*. American Bureau of Shipping, Corporate Offshore Technology, Renewables. Houston, TX.

[30] Hasselmann K, Barnett TP, Bouws E et al. 1973 Measurements of wind wave growth and swell decay during the Joint North Sea Wave Project (JONSWAP). *Deut. Hydrogr. Zeit*, A8, 1-95.(http://resolver.tudelft.nl/uuid:f204e188-13b9-49d8-a6dc-4fb7c20562fc)

[31] Van der Tempel J., Molenaar D.P. 2002 Wind Turbine Structural Dynamics – A Review of the Principles for Modern Power Generation, Onshore and Offshore. *Wind Eng.* **26**(4), 211-220. (doi: 10.1260/030952402321039412)

[32] Manwell JF, McGowan JG, Rogers AL. 2010 *Wind energy explained: Theory, design and application*. Chichester, UK: John Wiley & Sons.

[33] Chakrabarti SK. 1987 *Hydrodynamics of offshore structures*. Southampton, UK: WIT Press.

[34] Witcher D. 2005 Seismic analysis of wind turbines in the time domain. *Wind Energy* **8**, 81-91. (doi: 10.1002/we.135)

[35] Valamanesh V, Myers AT. 2014 Aerodynamic damping and seismic response of horizontal axis wind turbine towers. *J. Struct. Eng.*, in press. (doi: 10.1061/(ASCE)ST.1943-541X.0001018).

[36] Seidel M, Foss G. 2006 Impact of different substructures on turbine loading and dynamic behaviour for the DOWNVInD Project in 45m water depth. In: *Conf. Proc.* EWEC 2006. Athens 2006.

[37] Mostafa YE, El Naggar MH. 2004 Response of fixed offshore platforms to wave and current loading including soil–structure interaction. *Soil Dyn. Earth. Eng.* **24**, 357-368. (doi:10.1016/j.soildyn.2003.11.008)

[38] Kuhn M. 2001 Dynamics and design optimisation of offshore wind energy conversion systems. Report no. 2001.002. Delft University Wind Energy Research Institute (DUWIND). (http://resolver.tudelft.nl/uuid:adc3b032-3dde-4e32-84c3-7b8e181e526)

[39] Carswell W, Arwade SR, DeGroot DJ, Lackner MA. 2014 Soil-structure reliability of offshore wind turbine monopile foundations. *Wind Energy*, in press. (doi: 10.1002/we.1710)

[40] Bhattacharya S, Adhikari S. 2011 Experimental validation of soil–structure interaction of offshore wind turbines. *Soil Dyn. Earth. Eng.* **31**, 805-816. (doi:10.1016/j.soildyn.2011.01.004)

[41] Bhattacharya S, Nikitas N, Garnsey J, Alexander NA, Cox J, Lombardi D, Muir Wood D, Nash DFT. 2013 Observed dynamic soil–structure interaction in scale testing of offshore wind turbine foundations. *Soil Dyn. Earth. Eng.* **54**, 47-60. (doi: 10.1016/j.soildyn.2013.07.012)